Western and Clark's grebes use novel strategies for running on water

Western and Clark's grebes use novel strategies for running on water

Glenna T. Clifton[1], Tyson L. Hedrick[2], Andrew A Biewener[1]

[1]Concord Field Station, Department of Organismic and Evolutionary Biology, Harvard University, Bedford, MA 01730

[2]Department of Biology, University of North Carolina at Chapel Hill, Chapel Hill, NC 27599

Research Article submitted to *The Journal of Experimental Biology*
February 16, 2015

Corresponding Author:

Glenna Clifton
Concord Field Station
100 Old Causeway Road
Bedford, MA 01730
gclifton@fas.harvard.edu

Running Title: Water running strategies in grebes

Keywords: Western Grebe, Clark's Grebe, kinematics, biomechanics, water, running

Word Count: 6549

Abstract

Few vertebrates run on water. The largest animals to accomplish this feat are Western and Clark's grebes (*Aechmophorus occidentalis* and *clarkii*). These birds use water running to secure a mate during a display called *rushing*. Grebes weigh an order of magnitude more than the next largest water runners, basilisk lizards (*B. basiliscus*), and therefore face a greater challenge to support their body weight. How do these birds produce the hydrodynamic forces necessary to overcome gravity and sustain rushing? We present the first quantitative study of water running by grebes. High-speed video recordings elucidate the hindlimb movements of grebes rushing in the wild. We complement these findings with laboratory experiments using physical models and a preserved grebe foot to estimate how slapping the water surface contributes to weight support. Our results indicate that grebes employ three novel tactics to successfully run on water. First, rushing grebes use exceptionally high stride rates, reaching 10 Hz. Second, grebe foot size and high water impact speed allow grebes to generate up to 30-55% of the required weight support through water slap alone. Lastly, flattened foot bones reduce downward drag, permitting grebes to retract each foot from the water laterally. Together, these mechanisms outline a water running strategy qualitatively different from that of the only previously-studied water runner, the basilisk lizard. The hydrodynamic specializations of rushing grebes could inform the design of biomimetic appendages. Furthermore, the mechanisms underlying this impressive display demonstrate that evolution can dramatically alter performance under sexual selection.

Introduction

Only a few animals are capable of running on water. Vertebrates are too dense to support their body above the water surface using surface tension alone, and must instead generate sizable hydrodynamic forces to water run. Under these circumstances, body mass plays a primary role in determining the difficulty of this feat. Yet, the largest animals capable of running on water, Western and Clark's grebes (*Aechmophorus occidentalis* and *A. clarkii*), have never been quantitatively studied. These birds water run during a pair bonding display called *rushing*. An order of magnitude heavier than the next largest water runners, basilisk lizards (*B. basiliscus*; Glasheen and McMahon, 1996a), rushing grebes are an untapped resource for studying the mechanisms used to successfully run on water.

Most animals that locomote on water are small insects, whose long limbs deform the water surface to generate surface tension forces capable of supporting their body weight (Hu and Bush, 2010). Larger animals would need unfeasibly long legs to use this mechanism (Baudoin, 1955). Instead, these animals locomote at the water surface by driving their legs into and through the water with enough power to produce other hydrodynamic forces, resulting from inertial impulses, fluid drag, and added mass (Bush et al., 2006). Unlike forces generated on solid ground, these fluid forces depend on an object's velocity and shape. Both of these aspects are constrained in large water running animals. Muscle power and contraction velocities limit the speed at which an animal can move its hindlimb through water (Hill, 1950). Foot sizes that maximize supportive hydrodynamic forces might also produce downward drag during limb retraction or impede movements during other forms of locomotion (Raikow, 1973; Richards and Clemente, 2013). The challenge of these requirements prohibits most animals, including humans, from running on water (Glasheen and McMahon, 1996a; Minetti et al., 2012). Among vertebrates, the only true water runners that have been studied are the basilisk lizards.

Western and Clark's grebes are arguably more successful at running on water than basilisk lizards. The much heavier grebes, weighing between 700 and 1800 g (Vuilleumier, 2009), must produce larger hydrodynamic forces than those of basilisk lizards to sustain water-running. Moreover, basilisk lizards experience a limit on their capacity to water-run with increased body size (Hsieh 2003; Glasheen and McMahon, 1996c). Adults struggle to stay above the water, often sinking after just a few steps. In contrast, a size-dependence on rushing ability has never been observed in grebes, and even the largest birds accomplish rushing bouts that last

several seconds and dozens of steps. Lastly, most basilisk lizards initiate water-running from land or nearby branches (Rand and Marx, 1967), whereas grebes start rushing from within the water. Grebes must accelerate their body out of the water and against water resistance, requiring the production of hydrodynamic forces greater than their body weight, *without* the use of their wings. These observations indicate that grebes outperform basilisk lizards at water running on multiple levels. Grebes are thus an interesting system in which to study effective locomotion at the water surface. Furthermore, the tactics that grebes use to support heavy weights during water running is particularly relevant for applications where weight minimization is a consistent challenge, such as robotics.

Rushing is more than an athletic achievement for Western and Clark's grebes. During the spring breeding season, grebes perform rushing to attract a mate and reinforce pair bonding. Each display consists of two or more grebes propelling themselves out of the water to run atop the surface. The wings of each bird are held still behind the body, and likely do not contribute to weight support. Rushing displays typically cover between 5-20 m and can last up to seven seconds (Nuechterlein and Storer, 1982). Although obviously a representation of strength and stamina, the qualities of rushing associated with female choice have yet to be identified. Rushing takes place throughout the breeding season, but decreases in regularity once most birds pair up and begin preparing for young.

For rushing grebes to successfully stay above the water, the forces produced during each stride must fully counteract gravity. Following the classification used for basilisk lizards (Glasheen and McMahon, 1996a), there are two main stride phases that generate supportive hydrodynamic forces: water slap and stroke. The extent that slap and stroke contribute to overall body weight support varies with size in basilisk lizards. Previous studies that quantify weight support in basilisk lizards focus on the generation of upward impulses, a measurement that incorporates both the magnitude of supportive forces and the time over which they are exerted. In small lizards (<10 g), slap impulses account for up to 60% of weight support, whereas they account for only 25% in large lizards (Glasheen and McMahon, 1996c). Consequently, larger lizards must derive a greater percentage of weight support from stroke phases in order to resist sinking. Weighing even more than basilisk lizards, do grebes also experience a reduction in the extent that slap contributes to weight support? What mechanisms do grebes use to produce enough force to sustain rushing?

This study quantitatively analyzes the rushing behavior of Western and Clark's grebes for the first time. Using high-speed cameras, we film grebes in the wild and describe the behavioral and kinematic characteristics of successful water running. To further investigate the force contribution of water slap, we modify a classic experiment to determine the upward impulse generated by model grebe feet in comparison with a freshly preserved grebe foot specimen. Our results reveal that rushing grebes employ a previously unidentified water-running mechanism that involves (1) using exceptionally high step rates, (2) producing large supportive slap forces with lobate feet, and (3) retracting the feet laterally from the water. Our findings provide new insight into the requirements for running at the water surface.

Results

Throughout the 2012 breeding season, the density of Western and Clark's grebes on Upper Klamath Lake increased and the abundance of rushing displays peaked, sometimes with over 30 displays per hour. Rushing was unaffected by weather conditions or wind speeds. The highest densities of displays occurred in early morning and midday, and were often initiated by environmental disturbances (such as loud passing aircraft or boats). Rushing would repeatedly occur in bouts, with one group displaying numerous times in succession and triggering displays in other groups.

Stride duration and frequency

We calculated stride duration using high-speed video recordings from 40 occurrences of grebe rushing. Rushing displays typically last 4 s, but range up to 7 s (Neuchterlein and Storer, 1982). The data capacity for the high-speed cameras limited each trial to 1.7s at 325 fps. Therefore, each filmed trial only recorded a section of the full display. For all trials, stride duration ranged between 0.10 and 0.15 s, corresponding to stride frequencies between 10 and 6.7 strides per second (Fig. 1). Because each rushing stride consists of two steps, our observed stride duration range corresponds to step frequencies between 20 and 13.3 steps per second. As the birds rise out of the water during rush initiation, stride duration is low and typically reaches a minimum within the first 10 steps (Fig. 1A). Stride duration decreases as grebes continue rushing (Fig. 1B). Some birds exhibit variability in stride duration throughout rushing; however, this

variation does not appear to be linked to weather or water conditions. To terminate rushing, grebes lean forward from their upright rushing posture and dive into the water. Regardless of the absolute stride duration at rushing termination, all birds show a successive increase in stride duration during the final 3-5 steps (Fig. 1C).

Rushing speed

Due to a challenging field environment, only a small fraction of our recordings were suitable for calibration and kinematic analysis (see *Methods* for more detail). The suitable recordings are an unbiased, random sampling of all rushing trials. Despite our small sample size, the findings from each trial are consistent.

For eight rushing trials, two calibrated camera views were used to analyze the speed of rushing grebes. The tip of each bird's beak was used as a proxy for whole body movement since grebes hold their neck still throughout rushing (see supplementary movie S1). The speed in the water-surface plane typically ranged between 1.5 and 4 m/s (Fig. 2). In all trials, the speed of both rushing birds was closely matched. When rising out of the water to begin rushing, translational speed was relatively high and remained mostly constant for at least one second (Fig. 2A). This high speed coincided with low stride durations. However, speed decreased steadily as rushing progressed, accompanied by an increase in stride duration (Fig. 2B). None of the calibrated trials showed rush termination. Overall, grebes began rushing with a high translational speed then, in coordination with their rushing partners, slowed down throughout the rest of the display.

Rushing hindlimb kinematics

In two trials, the distal hindlimb was digitally tracked for a total of 13 strides. Data completeness for each stride varied greatly due to bird orientation, water splash, and movement inconsistencies. Despite this variation, all strides showed the same qualitative patterns (Fig. 3C,D,E). Each stride can be divided into two sections: foot submersion (Fig. 3C,D; outlined green triangles) and swing (filled-in green triangles). Submersion includes propulsive phases, slap and stroke, as well as foot retraction. Swing is defined as the time when the entire foot is removed from the water. The beginning of water slap marks the transition from swing to submersion.

Throughout the stride, the distal hindlimb moves in a stereotyped pattern. The intertarsal "ankle" joint (green triangle) makes a slight vertical arc but moves principally in the travel direction of the bird (Fig. 3C,D). The metatarsophalangeal joint (MTP, red square) is retracted obliquely out of the water, making a broad vertical and medial arc. After reaching its most vertical position, the MTP briefly swings laterally then returns medially during the foot's final descent before slap (Figs 3D, 4B). At the time of slap, the MTP is medial with respect to the ankle (Fig. 4B). The distal aspect of each digit was tracked; however, the lobate digits (Fig. 3B) are collapsed together throughout most of swing, only spreading during the final 15-20 ms before slap. The location of digit IV therefore represents the movement of all digits for the first ¾ of swing. During foot retraction, the digits are tucked tightly behind the tarsometatarsus. As the MTP travels medially, the digits swing laterally and remain at a fairly constant vertical height (Figs 3C, 4A). Before descending for slap, the digits begin traveling medially and reach their most vertical excursion.

During the final six frames of swing (approximately 18ms), the foot descends and the toes spread in preparation for water slap. The ankle makes a small inferior and lateral excursion (Fig. 3C,D). The MTP and digits undergo coordinated mediolateral movements while descending, resulting in toe spreading. At the beginning of descent, the MTP has already traced a small lateral arc and the folded digits remain lateral to the MTP. The folded digits accompany the MTP as it swings medially; however, the digits undergo a larger excursion and reach a more medial position (Fig. 4B, arrow). During the final 3-4 frames, the digits separate as digit IV then digit III swing laterally (Fig. 3E). At the time of slap, the digits are completely spread with digits II and III medial to the MTP. The velocity of the foot at the time of slap was calculated using the MTP vertical speed during three frames prior to slap. For 13 strides, the foot slap velocity was 3.83 ± 0.65 (s.e.) m/s.

Vertical impulse from water slap

To further understand the forces produced while rushing, a classic laboratory experiment (Glasheen and McMahon, 1996b,c) was reproduced and then analyzed in reference to the slap impact velocity observed for wild grebes (see *Materials and Methods*). We found that the slap impulse of model grebe feet and a preserved grebe foot depends both on impact velocity and foot area (Fig. 5). Slap impulses generated by the preserved grebe foot (34.2 cm^2) relative to the large

(34.3 cm^2) foot model were slightly larger, but not significantly different (p=0.77, see *Materials and Methods*), suggesting that the small difference may depend on the intrinsic compliance of the preserved grebe foot relative to the rigid foot model. The experimental slap impulses for the models and preserved grebe foot increased with impact velocity. The relationship between slap impulse and impact velocity is best described using a quadratic regression (large model: R^2= 0.98; large preserved: R^2 = 0.95; small model: R^2 = 0.99; see *Materials and Methods*). The larger model foot and preserved grebe foot produced greater slap impulses than the small model foot.

For a bird with each foot size, the theoretical minimum impulse needed to resist sinking was calculated using the mass of the associated carcass (small: 0.78 kg, large: 1.44 kg) and a maximum stride frequency of 10 Hz obtained from field trials (see Eq. 1 in Methods). The calculated minimum needed impulses (small: 0.38 N*s, large: 0.71 N*s) were used to convert the experimental slap impulses into a percentage of what would be needed to stay above water. Within the range of average foot slap velocities observed in field trials, our laboratory-based foot slaps produced between 35-55% (small foot) and 30-50% (large model and cadaver feet) of the impulse needed to support a grebe's body weight (Fig. 5). While the larger feet produced a greater magnitude slap impulse, its relative contribution to body weight support is less than for the smaller foot model.

Discussion

For the first time, we filmed and quantitatively analyzed the rushing behavior of the heaviest known water runners, Western and Clark's grebes. Due to their relatively heavy weights, these birds must produce the largest hydrodynamic forces of any known water running animal. We analyzed numerous rushing displays during the spring 2012 breeding season to determine how these birds produce the forces necessary to sustain rushing. We find three primary elements that contribute to a grebe's ability to successfully run on water: high stride rate, high slap force production, and drag reduction during foot retraction.

Stride Rate

During rushing, grebes use the highest stride rate recorded for any previously-studied, running bird. Rushing grebes take between 14 and 20 steps per second, a stride frequency of 6.7

to 10 Hz (Fig. 1). This stride rate equals that of the basilisk lizard (Glasheen and McMahon, 1996c), and is much higher than expected for an animal of a grebe's size. Theoretical biomechanical models assuming dynamic similarity predict that stride frequency should scale inversely with leg length, and therefore body size (McMahon, 1975; Alexander and Jayes, 1983; Biewener, 2003). This scaling relationship has been broadly supported in quadrupedal mammals (Heglund et al., 1974; Heglund and Taylor, 1988; Iriate-Diaz, 2002). Although less extensively studied in bipeds, inverse scaling of stride frequency with body mass holds for several running birds and humans (Gatesy and Biewener, 1991). This work indicates that the heavier grebes should run with lower stride frequencies than basilisk lizards, but in fact they actually use equal rates. Additionally, bipedal running birds with comparable masses to grebes, namely guinea fowl, run with lower maximum stride frequencies: 3.2 strides per second on a treadmill (Gatesy and Biewener, 1991) or 4.0 strides per second in the wild (Maloiy et al., 1979). Compared to running birds of a similar size, grebes rush with a much higher stride rate. In fact, we were unable to find a record of a higher stride rate used by any bird.

A high stride rate is critical for grebes to run on water. For a set amount of force that a single step can produce, an increased stride rate allows that force to be generated more often, directly boosting total force production over a given period of time. While forces could also be augmented through modifications in grebe foot anatomy, these changes are likely to have broad impacts on other aspects of grebe behavior. Larger feet would increase their mass inertia and might therefore limit stride rate. Altering stride frequency faces fewer constraints, and is an effective way for grebes to increase body weight support at the water surface.

Because the stride rate of a water runner directly influences how much force is generated over time, it makes sense for grebes to adjust running frequency based on force requirement. Various rushing phases (e.g. initiation) necessitate differing magnitudes of supportive force. Grebes begin rushing with a very high stride frequency, which then decreases throughout the rest of the display (Fig. 1). The difficulty of accelerating the body out of the water could account for the peak stride frequency observed at the beginning of rushing. Throughout the remainder of a rushing display, translational speed decreases, accompanied by a decrease in stride rate (Fig. 2). This link suggests that grebes use stride frequency to regulate force production throughout rushing.

Slap Impulse Production

Compared to adult basilisk lizards, Western and Clark's grebes obtain approximately twice as much relative weight support from slapping the water surface. Our laboratory experiments suggest that slap phase during grebe rushing accounts for 30-55% of the impulse needed for weight support (Fig. 5), whereas slap in basilisk lizard water running only contributes 15-30% (Glasheen and McMahon, 1996c). Our results comparing rigid large and small model feet with a slightly smaller taxidermically prepared and mounted grebe foot show that the intrinsic compliance of actual grebe feet only slightly influences the slap impulse generated. In order to sustain rushing, the total impulse generated from each step--including both its slap and stroke phase--must be equal to or greater than the gravitational impulse acting on the bird during that time. By generating larger relative slap impulses, grebes relax constraints on stroke impulse, and make whole-body weight support more attainable.

During water slap, both small and large grebe feet contribute similarly to weight support, a trend distinct from the size-dependent impulse production observed in basilisk lizards. While smaller grebes generate slightly higher relative slap contributions than larger grebes (35-55% vs. 30-50% respectively), the observed difference is much less than that seen in basilisk lizards. Basilisk lizards weighing less than 10 g produce up to 60% of weight support through water slap, whereas adults weighing above 150 g are restricted to 10-25% (Glasheen and McMahon, 1996c). This discrepancy corresponds to variations in water running success. Juvenile basilisk lizards generate force surpluses exceeding 50% of their body weight (Hsieh and Lauder, 2004), but large adults barely overcome gravity even when producing maximal forces (Glasheen and McMahon, 1996c). In comparison, both small and large grebes produce relative slap impulses similar to those of juvenile basilisk lizards. The slap impulses that all rushing grebes generate correspond to those of only the smallest, and most able, basilisk lizards.

High slap force production by rushing grebes may result from their unusual foot shape and fast slap velocity. Hydrodynamic forces acting on an object predominantly rely on its size, shape, and velocity. When compared to basilisk lizards, grebe foot size alone does not account for their enhanced slap force contribution. Using an experimentally-derived scaling relationship between basilisk lizard body mass and foot area (Glasheen and McMahon, 1996c), the foot area of a grebe-sized basilisk lizard would be 19 or 27 cm^2 for a small and large grebe respectively. Actual grebe feet are only 25% larger than scaled basilisk lizard feet, at 24 and 34 cm^2. The

relationship between area and slap impulse has not been experimentally measured for complicated foot shapes. However, simpler shapes have been examined. Circular discs dropped into water produce slap impulses directly proportional to the mass of a sphere of water with the same radius as the disc, its virtual mass (Glasheen and McMahon, 1996a). Therefore, the slap impulse scales with (disc area)$^{3/2}$. If we assume that grebe feet behave like circular discs, a 25% increase in area only produces a 40% increase in slap impact, not enough to account for the 100% gain observed. Instead, other factors likely contribute to a grebe foot's ability to produce hydrodynamic forces during water slap. First, the feet of all grebes are uniquely lobate, a shape that has been proposed to function as lift-producing airfoils during underwater swimming (Johansson and Norberg, 2000). This shape may benefit rushing grebes by generating larger slap forces. Second, rushing grebes strike the water surface at high impact velocities (v_{impact}) reaching up to 4.5 m/s. In comparison, basilisk lizards slap the water surface at a peak velocity of 3.75 m/s (Glasheen and McMahon, 1996b; Hsieh, 2004). Because hydrodynamic forces increase with velocity squared (v_{impact}^{2}), even a modest 20% increase of impact velocity in grebes would amplify slap impulse by 44%. While size, shape, and velocity may all contribute to observed increases in grebe slap impulse, foot size and slap impact velocity are likely most important.

Drag Reduction

To successfully run on water, an animal must not only produce supportive, upward forces, but also minimize any downward forces that might induce sinking. These downward forces primarily result from drag acting on the feet during their retraction from the water. As an animal pulls its foot upward, hydrodynamic drag acts to pull the animal down. Therefore, reducing drag production during foot retraction mitigates the necessary supportive forces for staying above the water.

Grebes retract their feet from the water laterally, indicating that they use a different drag reduction mechanism than basilisk lizards. A critical aspect of water running in basilisk lizards involves retracting the feet through air cavities formed during underwater stroke (Glasheen and McMahon, 1996a,c). Air has a lower mass density than water, and therefore imposes less resistive drag. As a basilisk lizard slaps the water and pushes its foot downward, an air bubble forms behind the foot. Missile drop experiments on basilisk lizard feet indicate that foot size determines the time it takes for the cavity to seal and collapse (Glasheen and McMahon,

1996a,c). To reduce drag, basilisk lizards retract each foot through the air bubble before its collapse. To do so, basilisk lizards retract their feet underneath their body (Hsieh, 2003). Grebes, however, use a different movement during foot retraction: the metatarsophalangeal joint makes a broad arc out of the water, exiting the water lateral to the bird (Figs 3C, 4A). Because grebes still slap the water surface medially under the body, a lateral foot retraction prohibits them from utilizing an air cavity. While it is unknown why grebes would use a lateral retraction, this movement might reflect a constraint on the underwater stroke foot motion. Diving grebes use a medially directed power stroke to produce lift (Johansson & Norberg, 2001). Rushing grebes may use a similar tactic to support their body weight, necessitating a lateral retraction of the foot out of the water. Regardless of its potential benefit, the lateral retraction observed during rushing suggests that grebes do not use the same air-cavity tactic as basilisk lizards for reducing drag during foot retraction.

Without the use of an air cavity, rushing grebes must either produce enough upward force to overcome any downward drag or use a unique drag reduction technique. One possibility for the latter could relate to the unusual structure of grebe feet, which become streamlined when collapsed. Grebe feet are compact while exiting the water, with the lobate toes folded together and curled behind the tarsometatarsus (TMT). Although we observed relatively small effect of foot compliance of actual grebe feet in comparison with rigid physical models (Fig. 5), the intrinsic compliance of grebe feet likely facilitates digit collapse and overall compression of the foot as a whole. This collapsed orientation also results from specialized foot joints. In grebes, the interphalangeal and MTP articulations allow each digit to rotate when it reaches a flexion of 90° (Stolpe, 1935). The folded digits lie underneath the plantar edge of the TMT. Unlike in most birds, the TMT in grebes is flattened medio-laterally with a relatively thick dorsal edge and tapered plantar edge. A coronal section of the TMT resembles an airfoil with a fineness ratio of 3.3 (Johansson & Norberg, 2001). Together, the TMT and folded toes reduce the cross-sectional area of the foot profile and form a streamlined shape. During retraction, the collapsed grebe feet move in line with the reduced cross-sectional area of the foot profile. The coordination of the limb movements with the collapse of the feet indicates that rushing grebes likely utilize the specialized anatomy of their feet to reduce drag.

Applications and Conclusions

The difficulty and rarity of water running makes it of high interest in several fields. At least two water running robots have been developed based on the basilisk lizard (Floyd et al., 2006; Xu et al., 2012). By altering the foot design (Floyd et al., 2008a), number of limbs (Floyd and Sitti, 2008b), and tail type (Park et al., 2009) these robots can travel up to 1.2 m at the water surface. Yet, current designs are energetically expensive and can only transition to terrestrial locomotion using footpad designs suboptimal for swimming (Park and Sitti, 2009). The water running mechanisms used by rushing grebes could provide inspiration for additional amphibious robots. Furthermore, the efficiency with which grebe feet produce upward forces suggests that grebes could serve as important models for the design of commercial and industrial products, such as paddles.

In summary we find that that, in comparison to basilisk lizards, Western and Clark's grebes use three novel mechanisms for running at the water surface. First, rushing grebes take up to 20 steps per second, corresponding to a stride frequency of 10 Hz that is higher than any previously studied running bird. Second, lobate toes and a high impact velocity of the feet allow grebes to generate up to 55% of the force needed to stay above water through slapping the water surface. Lastly, grebes retract their feet laterally, using flattened foot bones and unique distal joint articulations to reduce downward drag. These findings present new insight into the requirements for successfully running on water and help elucidate the complicated hydrodynamics of the air-water boundary. As the largest animals capable of water running, Western and Clark's grebes are likely the best models for human-fabricated designs that produce large forces at the water surface.

Materials and Methods

Field Recordings

Western and Clark's grebes perform rushing in order to select a mate for the breeding season. As a pair bonding display, rushing cannot be elicited in a laboratory setting. Instead, studying this behavior requires observing grebes in their natural environment. The highest density of breeding Western and Clark's grebes occurs in the Pacific Northwest. We filmed rushing grebes at Putnam's Point of Upper Klamath Lake (Klamath Falls, Oregon) during May of 2012. Wind speed and weather conditions were recorded at the time of each trial.

Rushing was filmed using two high-speed cameras (NR5S1, Integrated Design Tools, Tallahassee, FL, USA). The cameras were placed 43.9 m apart on the south shoreline of Upper Klamath Lake (Fig. 6A). Each camera set-up included a 300 mm zoom lens (70-300 mm, Nikon), a 1.4x teleconverter (420 mm equivalent focal length), and a circular polarizing filter (62 mm). Recordings were collected using Motion Studio Software at 325 frames per second with a resolution of 2336x1728 pixels.

Filming a rushing bout was an unpredictable and involved process. At any point in time, between 20 and 200 grebes were present in the observable range of the cameras, typically within 50 to 150 m from the cameras. Rushing grebes began showing pre-rushing behaviors 3-8 seconds before rushing initiation (Nuechterlein and Storer, 1982). Both cameras were manually repositioned, zoomed, and focused on grebes expected to begin rushing. For each rushing trial, the cameras were post-triggered and recorded a maximum of 572 frames, equivalent to 1.7 seconds. The distance from each camera to the rushing site was estimated using a laser rangefinder (Bushnell Sport 850, Bushnell Outdoor Products, Overland Park, Kansas, USA). We filmed more than 100 trials in total. We approximate that we witnessed over 1000 rushing displays throughout the month. The trials we filmed represent a random sampling due to filming conditions, and likely do not represented a biased resampling of individuals.

Un-calibrated Trials

Twenty of the most focused and zoomed-in rushing trials were analyzed for stride duration. This included 40 birds, with one to three grebes per trial. The stride duration was defined as the time between successive water slaps by the same limb, using the onset of submersion as the indicator of slap. The number of frames between slap was converted to duration (1 frame ~ 3.07 ms) and instantaneous frequency (freq = duration^{-1}). Each trial was identified as rushing initiation, steady rushing, or rushing termination.

Calibrated trials

Deriving quantitative spatial information from a rushing trial requires additional camera calibration recordings and analysis. When completed, calibration allows triangulation of a three-dimensional (3D) location from two-dimensional locations identified in the grebe video images. In this case, calibration was performed by moving an object of known length (a calibration wand) through the field of view of the cameras. An 86 cm wand was attached to a remote control

boat, which was then driven through the camera view following a rushing recording. Camera calibration was performed using the easyWand MATLAB (The Mathworks, Natick, MA, USA) routine (Therialt et al., 2014) using the wand information and known camera intrinsic parameters for the principal point and focal length. In addition to the wand length, calibrations were validated by computing the distance between the two cameras and comparing it to the value measured in the field for each recording. The resulting calibration was aligned to the water surface with additional custom MATLAB routines and the final calibration expressed as a set of direct linear transformation coefficients facilitating data analysis using the DLTdv5 MATLAB routine (Hedrick, 2008). Due to the unpredictable location of rushing events, re-calibration of the cameras was required for every trial.

Only a small fraction of rushing trials depicted enough detail for analysis and satisfied the requirements for successful calibration. The difficulties of filming animals in the field limited the scope and quality of our data. Rushing occurred close to shore only a few times. The majority of our recordings captured grebes too far away for detailed study. Furthermore, the direction of rushing and water splash often obscured the view of the hindlimbs, preventing kinematic analysis. The calibration process posed additional challenges. Accurately transforming filmed data to 3D coordinates requires that: (1) both cameras remain perfectly still throughout recordings, (2) cameras do not shift between rushing and calibration recordings, and (3) the calibration wand is recorded in enough locations to provide sufficient shared information among the two cameras. The windy and choppy field conditions as well as the need to rapidly reposition cameras in anticipation of a rushing event made it difficult to achieve the first and second criteria, while the remote boat method limited wand information to a ~1 m high region above the water surface, increasing the number of wand points required for a successful calibration.

Despite the challenges of filming rushing grebes in the wild, moving the calibration wand throughout the camera field of view, and achieving suitable camera conditions, eight trials were successfully calibrated, two showing hindlimb detail. These trials were random samples from all rushing trials and showed findings qualitatively consistent with each other. These data are therefore likely to adequately characterize rushing and represent a significant new achievement of obtaining quantitative high-speed three-dimensional kinematic data under field conditions.

Field Kinematics Analysis

Eight trials were successfully calibrated and 15 grebes were analyzed for whole body speed. The tip of each bird's beak was digitally tracked (Hedrick, 2008). Rushing grebes hold their head and neck still relative to their body, making the tip of the beak a good approximation of whole body movement. The x-y and z speed of each bird was calculated as the numerical derivative of the digitized beak position and was passed through a simple moving average filter using 20 points, corresponding to half of the average 40 frames per stride. Each trial was identified as either rushing initiation or steady rushing. No calibrated trials included rushing termination.

Two of the calibrated trials showed sufficient detail to be used for hindlimb kinematic analysis. In Western and Clark's grebes, the upper hindlimb is incorporated in the body musculature and the hip and knee joints are not identifiable. Therefore, the following skeletal landmarks were tracked: ankle joint, metatarsophalangeal joint (MTP), and distal phalanx of digits II-IV (Fig. 3A,B). These points were often only visible during swing, when the foot was completely removed from the water. During two strides, the ankle was visible for the entire stride. The x-axis was defined as the average travel direction of the bird's ankle joint throughout the digitized range. The y-axis represented the mediolateral plane of the bird, using the digitized points from both ankles. The z-axis was calculated from the cross product of x- and y-axes, representing the vertical axis of the bird relative with an origin at the water surface. Due to variation in the visibility of joints, kinematic data could not be quantitatively combined over multiple strides.

For two birds, the MTP joint was analyzed to calculate the velocity of the foot at water slap. The MTP impact velocity of 13 total slaps was calculated from the digitized MTP position data for 3 frames prior to slap. The slap velocity was averaged for each bird then combined to find the grand average and variance.

Slap Impulse Experiment Theory

Measurement of the hydrodynamic forces produced while rushing is not possible from the field kinematics. In order to elucidate the impulses that rushing grebes produce to support their body weight, we modified and replicated a classic laboratory experiment on the water slap of basilisk lizards (Glasheen and McMahon, 1996a,c).

The hydrodynamic impulses produced by irregularly shaped objects cannot be theoretically calculated and must be experimentally quantified. Following the model of Glasheen and McMahon (1996a,b,c), we estimate the contribution of water slap to full body weight support. Assuming that only one foot is submerged at a time and aerial phases are short or absent, the minimum impulse needed to fully support one's body weight ($\text{impulse}_{\text{needed}}$) is:

$$\text{impulse}_{\text{needed}} = M_b g \tau_{\text{step}} \quad (1)$$

where M_b is body mass (kg), g is gravitational acceleration (m/s^2), and τ_{step} is the period between consecutive foot slaps (s). To meet this impulse requirement and therefore resist sinking, water runners produce hydrodynamic forces during water slap and underwater stroke. Here, we focus on the slap phase because our field recordings do not allow for estimation of underwater movements of grebe feet. The impulse generated by a foot slapping the surface ($\text{impulse}_{\text{slap}}$) equals the mass of water accelerated by the slap multiplied by the slap velocity of the foot . From the conservation of momentum, slap impulse must also equal:

$$\text{impulse}_{\text{slap}} = M_{\text{foot}} \Delta u_{\text{slap}} \quad (2)$$

$$\Delta u_{\text{slap}} = u_{\text{impact}} - u_{\text{end}} \quad (3)$$

where M_{foot} is the foot mass (kg), u_{impact} is foot velocity at beginning of slap, and u_{end} is foot velocity at the end of slap phase.

Grebe Foot Model Design and Cadaver Preparation

Model grebe feet were designed using measurements from Western Grebe carcasses and 3D printed. Seven Western Grebe carcasses (mass = 0.7-1.4 kg) were obtained from rehabilitation centers and the limbs were measured and photographed. The area and dimensions of each foot was digitally calculated (ImageJ, NIH, Bethesda, Maryland, USA). A representative outline of a grebe foot (34.3 cm^2) was traced from a picture of the second largest grebe specimen. The outline was scaled to the calculated area of the second smallest (24.3 cm^2) specimen. A flat model of each outline was fabricated using a 3D printer (thickness = 1 cm). The hydrodynamic performance of the second largest grebe foot specimen (34.2 cm^2) was also tested by securing the freshly preserved foot in a taxidermically abducted position using Masters Blend (McKenzie Taxidermy Supply, Granite Quarry, NC).

Slap Impulse Experiment Set-up

The slap impulse of the small and large model grebe feet and the prepared grebe foot were measured using a laboratory set-up similar to that of Glasheen and McMahon (1996a,b,c). Model grebe feet were attached onto a 0.46 m "missile" of 80/20 aluminum stock (80/20 Inc., Columbia City, IN). The missile was attached onto a 1.52 m long, vertical 80/20 track using a linear motion fitting (Fig. 6B). The track enforced a consistent vertical drop of the foot into a water tank with a 0.366 m depth. The top of the missile was attached to a low stretch, Spectra string that was wrapped around a foam spool. The spool was directly attached to an analog optical encoder (E5, 900 CPR, US Digital, Vancouver, WA), which measured its angular velocity. This signal was converted to a measurement of the downward velocity of the foot. The optical encoder was calibrated by translating the missile at 6 known velocities using a linear actuator. A single-axis accelerometer (ADXL193, Analog Devices, Norwood, MA) was enclosed in a waterproof case and attached to the top of the missile. The optical encoder and accelerometer outputs were sampled at 100 kHz.

Using this set-up, the model feet and cadaveric foot were dropped into the water from varying heights (0.04-1.5 m) for a total of 90 trials each. The attachment angle of the cadaveric foot imposed a lower limit on drop height, precluding trials for the lower impact velocity range. Any trials with irregularities in the optical encoder output were excluded. The mass of the missile, M_{foot}, was weighed before every trial to account for water retention within the missile and string. Timing of slap phase was found from the accelerometer trace. For each trial, the beginning of slap, t_{slap}, was defined as the last data point within one standard deviation of the average free fall acceleration (Fig. 1C). For the model feet, the end of slap, t_{end}, was determined as the time of maximum acceleration after slap began. Because the attachment of the taxidermically prepared grebe foot prevented the missile from slapping the water surface perpendicularly, the time of slap was prolonged and determined by finding when the derivative of the filtered acceleration trace was positive for the next 300 frames (0.52 second). This threshold was chosen since it consistently corresponded to the inflection point for the integrated velocity as shown in Glasheen & McMahon (1996a, Fig 1A). The optical encoder velocity data for both model feet and the preserved grebe foot was passed through a moving average filter (n=5), and the resulting trace, u_{OE}, was used to find the foot velocity at slap impact, u_{impact}. The integrated accelerometer output, u_a, was calibrated such that $u_a(t_{slap}) = u_{impact}$. The change in velocity during slap was calculated as:

$$\Delta u_{\text{slap}} = u_{\text{impact}} - u_{\text{end}} \tag{4}$$

where u_{end} is the velocity at end of slap. The fraction of needed impulse obtained from slapping the water surface was found by:

$$\text{fraction of needed impulse} = \frac{M_{\text{foot}} \Delta u_{\text{slap}}}{\text{impulse}_{\text{needed}}} \tag{5}$$

$\text{Impulse}_{\text{needed}}$ is calculated using (1) with a τ_{step} of 0.05 s, corresponding to an upper bound in stride frequency of 20 Hz, and an M_{b} corresponding to that of the foot model. The body mass associated with each model foot size--0.78 and 1.44 kg for small and large, respectively--was estimated as the body mass of the carcass with the most similar foot area.

The experimental slap impulse data were fit using a nonlinear regression, y=*a**x^2, based on hydrodynamic theory (Shiffman & Spencer, 1945) and prior experimental support (Moghisi & Squire, 1981). To test whether the data for the large model foot differ from those for the large cadaver foot, we use a two-tailed t-test of the regression coefficient, *a* (MATLAB).

List of Abbreviations

a	acceleration output from accelerometer
Δu_{slap}	change in velocity during slap phase
$impulse_{needed}$	impulse needed to fully support a water runner's body weight
$Impulse_{slap}$	Impulse produced by slapping the water surface
M_b	body mass
M_{foot}	mass of foot
MTP	metatarsophalangeal joint
t_{end}	time of end of slap phase
t_{slap}	time of beginning of slap phase
τ_{step}	period between consecutive steps
TMT	tarsometatarsus
u_a	velocity from integrated accelerometer output
u_{end}	velocity at end of slap phase
u_{impact}	vertical velocity at impact
u_{OE}	velocity output from optical encoder

Acknowledgments

We are grateful to the Oregon Department of Fish and Wildlife, Klamath Basin NWR, Klamath Falls Audubon Society, and especially the Wenner family for their gracious assistance during our field study. We also thank Autumn Turner and Matthew Wysocki for help with field recordings, and Evan Bluhm (UNC) for assistance with the camera calibration operations. Lastly, we would also like to thank the personnel at the Concord Field Station, the 2013 Harvard OEB 210 class, and the Ornithology department at the Museum of Comparative Zoology, Harvard University.

Author Contributions

GTC collected data, performed experiments, analyzed data, and prepared the manuscript. TLH analyzed calibration data, provided guidance, and assisted with writing. AAB provided guidance throughout the study and assisted with writing.

Funding

This work was supported by the Robert A. Chapman Memorial Scholarship and Theodore H. Ashford Graduate Fellowships to GTC and National Science Foundation IOS-1253276 to TLH.

References

Alexander, R. and Jayes, A. (1983). A dynamic similarity hypothesis for the gaits of quadrupedal mammals. *J. Zool.* 135–152.

Baudoin, R. (1955). La physicochimie des surfaces dans la vie des Arthropodes aeriens des miroirs d'eau, des rivages marins et lacustres et de la zone intercotidale. *Bull. Biol. Fr. Belg*. 89, 16–164.

Biewener, A. A. (2003). *Animal Locomotion.* Oxford, UK: Oxford University Press.

Bush, J. W. M. and Hu, D. L. (2006). WALKING ON WATER: Biolocomotion at the Interface. *Annu. Rev. Fluid Mech.* **38**, 339–369.

Floyd, S., Keegan, T., Palmisano, J. and Sitti, M. (2006). A Novel Water Running Robot Inspired by Basilisk Lizards. *2006 IEEE/RSJ International Conference on Intelligent Robots and Systems* 5430–5436.

Floyd, S. and Sitti, M. (2008). Design and development of the lifting and propulsion mechanism for a biologically inspired water runner robot. *IEEE Transactions on Robotics* **24**, 698–709.

Floyd, S., Adilak, S., Ramirez, S., Rogman, R. and Sitti, M. (2008). Performance of different foot designs for a water running robot. *2008 IEEE International Conference on Robotics and Automation* 244–250.

Gatesy, S. and Biewener, A. (1991). Bipedal locomotion: effects of speed, size and limb posture in birds and humans. *J. Zool.* **224**, 127–147.

Glasheen, J. and McMahon, T. (1996a). Vertical water entry of disks at low Froude numbers. *Phys. Fluids* **8**, 2078.

Glasheen, J. and McMahon, T. (1996b). A hydrodynamic model of locomotion in the basilisk lizard. *Nature* **380**, 340–342.

Glasheen, J. and Mcmahon, T. (1996c). Size-dependence of water-running ability in basilisk lizards (Basiliscus basiliscus). *J. Exp. Biol.* **199**, 2611–8.

Hedrick, T. L. (2008). Software techniques for two- and three-dimensional kinematic measurements of biological and biomimetic systems. *Bioinspiration Biomimetics* **3**, 1–6.

Heglund, N. and Taylor, C. (1988). Speed, stride frequency and energy cost per stride: how do they change with body size and gait? *J. Exp. Biol.* **138**, 301–318.

Heglund, N., Taylor, C. and McMahon, T. (1974). Scaling stride frequency and gait to animal size: mice to horses. *Science* **186**, 1112–1113.

Hill, A. V. (1950). The dimensions of animals and their muscular dynamics. Sci. Prog. Twent. Cent. **38**, 209-230.

Hsieh, S. T. (2003). Three-dimensional hindlimb kinematics of water running in the plumed basilisk lizard (Basiliscus plumifrons). *J. Exp. Biol.* **206**, 4363–4377.

Hsieh, S. T. and Lauder, G. V (2004). Running on water: Three-dimensional force generation by basilisk lizards. *Proc. Natl. Acad. Sci. U. S. A.* **101**, 16784–8.

Hu, D. L. and Bush, J. W. M. (2010). The hydrodynamics of water-walking arthropods. *J. Fluid Mech.* **644**, 5.

Iriarte-Díaz, J. (2002). Differential scaling of locomotor performance in small and large terrestrial mammals. *J. Exp. Biol.* **205**, 2897–908.

Johansson, L. C. and Norberg, U. M. (2000). Asymmetric toes aid underwater swimming. *Nature* **407**, 582–583.

Johansson, L. C. and Norberg, U. M. (2001). Lift-based paddling in grebes. *J. Exp. Biol.* **204**, 1687–1696.

Maloiy, G., Alexander, R., Njau, R. and Jayes, A. (1979). Allometry of the legs of running birds. *J. Zool.* **187**, 161–167.

McMahon, T. (1975). Using body size to understand the structural design of animals: quadrupedal locomotion. *J. Appl. Physiol.* **39**, 619–627.

Minetti, A. E., Ivanenko, Y. P., Cappellini, G., Dominici, N. and Lacquaniti, F. (2012). Humans running in place on water at simulated reduced gravity. *PloS One* **7**, 1-7.

Moghisi, M. and Squire. P.T. (1981). An experimental investigation of the inertial force of impact on a sphere striking a liquid surface. *J. Fl. Mech.* **108**, 133-146.

Nuechterlein, G. L. and Storer, R. W. (1982). The Pair-formation displays of the western grebe. *Condor* **84**, 351–369.

Park, H. S. and Sitti, M. (2009). Compliant footpad design analysis for a bio-inspired quadruped amphibious robot. *2009 IEEE/RSJ International Conference on Intelligent Robots and Systems* 645–651.

Raikow, R. (1973). Locomotor Mechanisms in North American Ducks. *The Wilson Bulletin* **85**, 295–307.

Rand, A. and Marx, H. (1967). Running speed of the lizard basiliscus basiliscus on water. *Copeia* **1967**, 230–233.

Richards, C. T. and Clemente, C. J. (2013). Built for rowing : frog muscle is tuned to limb morphology to power swimming. *J. R. Soc. Interface* **10**, 20130236.

Shiffman, M. and Spencer D.C. (1945). The force of impact on a sphere striking a water surface. Approximation by the Flow about a Lens. *App. Math. Panel, NDRC, Report 105.*

Stolpe, M. (1935). Colymbus, Hesperornis, Podiceps: ein Vergleich ihrer hinteren Extremität. *Journal fur Ornithologie* **83**, 115–128.

Therialt, D. H., Fuller, N. W., Jackson, B. E., Bluhm, E., Evangelista, D., Wu, Z., Betke, M., Hedrick, T. L. (2014). A method for accurate multi-camera field videography. *J. Exp. Biol.* **217**, 1843-1848.

Vuilleumier, F. (2009). *Birds of North America*. New York: Dorling Kindersley.

Xu, L., Wei, X., Cao, K. and Shi, Y. (2012). Dynamic analysis of fluid-structure interaction for the biped robot running on water. *International Conference on Control, Automation, Robotics & Vision* 1546–1550.

Figure 1

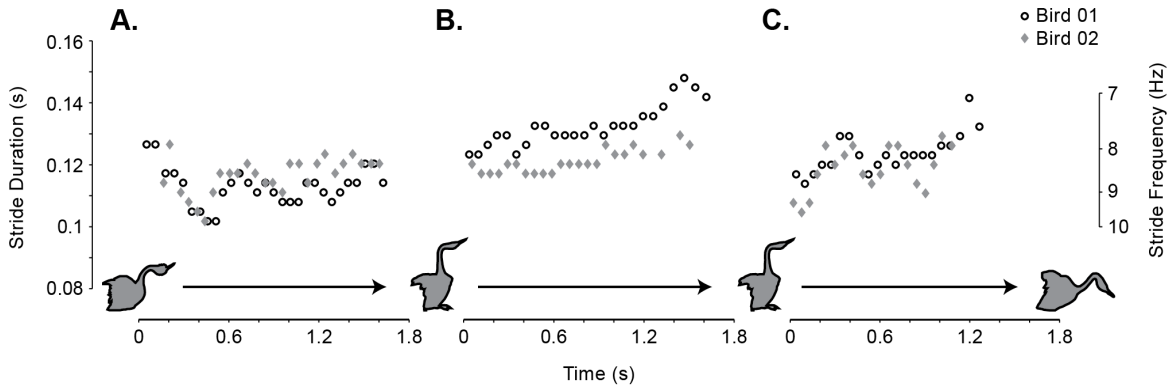

Figure 1. Stride duration and frequency during progressive stages of rushing. Each subplot shows a separate pair of grebes with open circles versus closed diamonds differentiating the two birds. (A) Stride duration decreases immediately (at 0.2 s) after rising out of the water then remains mostly constant. (B) Stride duration and frequency for a pair of grebes during the middle of a rushing display. Stride duration increases for both birds while rushing. (C) Stride duration and frequency for two grebes prior to ending a rushing display and diving into the water. One bird shows a fairly constant increase in stride duration before diving. The other bird's stride duration is more variable, but also increases during the final few strides.

Figure 2

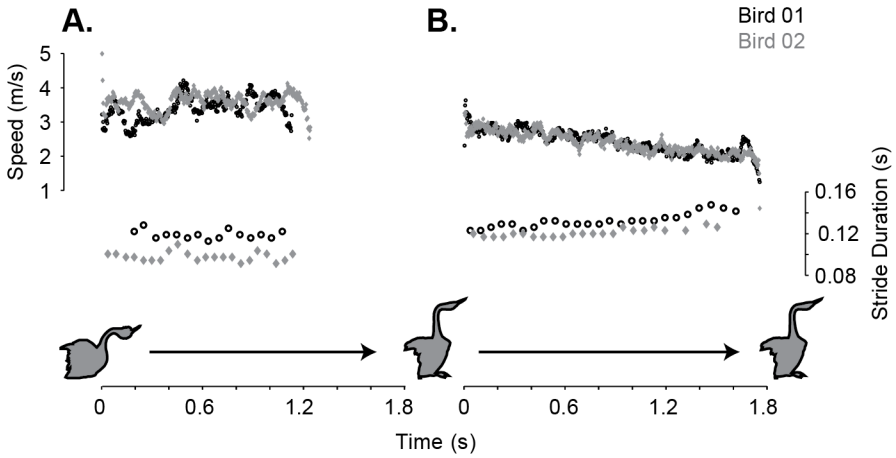

Figure 2. Speed and stride duration profiles for two grebes during beginning and middle of rushing. Due to the limited number of calibrated trials used to calculate speed, these profiles are not the same as those shown for stride duration (Figure 1). Speed was calculated as the numeric derivative of beak position and was passed through a simple moving average filter using 20 points, which relates to half of the average 40 frames per stride. (A) Two grebes rise out of the water and initiate rushing with relatively constant speeds and stride durations. Although the cameras could capture up to 1.76 seconds, these birds ran outside of the camera view after around 1.25 seconds. (B) Two grebes during the middle of rushing decrease speed and increase stride duration. No calibrated trials included grebes diving into the water after rushing.

Figure 3

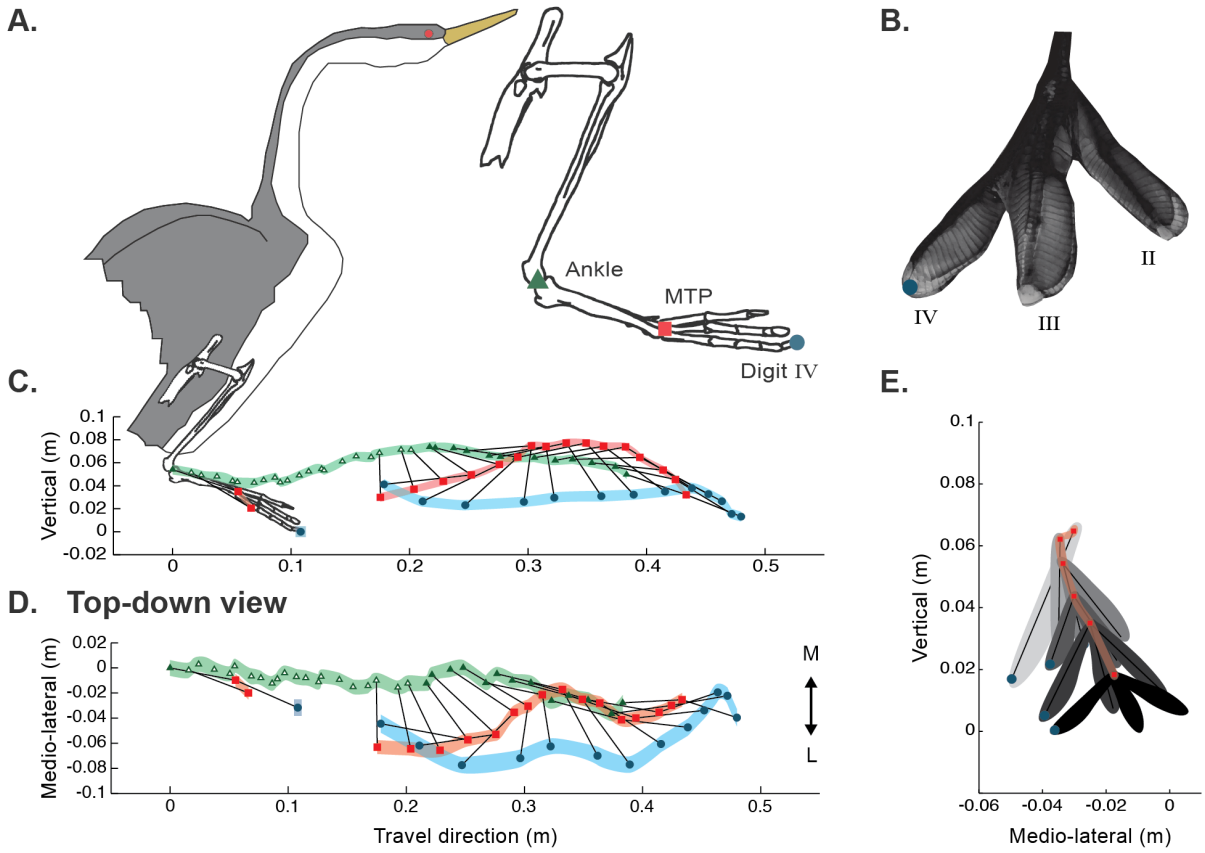
A.
Ankle
MTP
Digit IV
B.
II
IV
III
C.
Vertical (m)
0.1
0.08
0.06
0.04
0.02
0
-0.02
0
0.1
0.2
0.3
0.4
0.5
D. Top-down view
Medio-lateral (m)
0.02
0
-0.02
-0.04
-0.06
-0.08
-0.1
M
L
Travel direction (m)
E.
Vertical (m)
Medio-lateral (m)
-0.06
-0.04
-0.02
0

Figure 3. 3D kinematics of a complete rushing stride with respect to bird travel direction and vertical. (A) A diagram of *A. occidentalis* body posture during rushing and of the right hindlimb skeleton. The drawing of the skeleton (Museum of Comparative Zoology, Harvard University, specimen 342951) shows digitized locations for the ankle, metatarsophalangeal (MTP) joint, and distal phalanx of digit IV. (B) A detailed view of the asymmetrically-lobed digits of *A. occidentali*s (MCZ, specimen TBD). The hallux, digit I, is located on the palmar side of the foot. (C, D) Movement of the distal right hindlimb during one complete stride, as seen from (C) the right lateral side of the bird and (D) above the bird. Filled-in ankle points (green triangles) denote frames in which the foot is completely removed from the water; open ankle points are times during which part or all of the foot is submerged. The origin is located at the water surface vertically and at the initial ankle position for medio-lateral and travel directions. Light shaded lines represent 95% confidence intervals of marker position for the given calibration and digitized points. Black lines connect digitized joint positions in the same frame. (E) Details of foot spreading before water slap, as viewed from in front of the bird. Locations of digits II through IV were tracked using high-speed videography of rushing. The origin is consistent with that defined in (C, D). Shading gets darker with consecutive frames, ending with black during the final frame prior to surface slap.

Figure 4

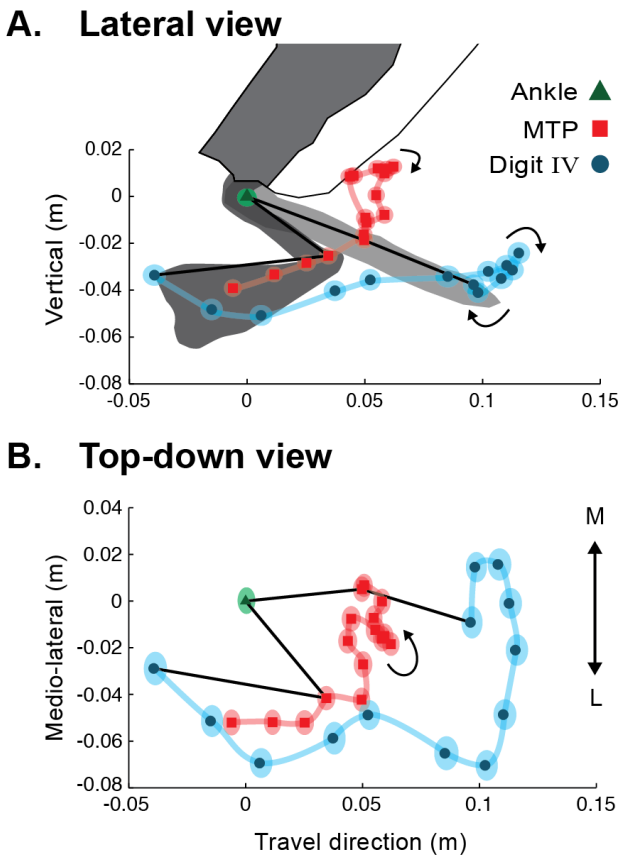

Figure 4. Movement of the MTP joint and digit IV relative to the ankle joint during swing. Trajectories of the right distal hindlimb are shown (A) from a lateral view and (B) from above the bird. Lightly shaded ellipses show the 95% confidence interval of the measurement in both directions for each point. Bolded lines denote the first frame with digit IV visible and the last frame before water slap.

Figure 5

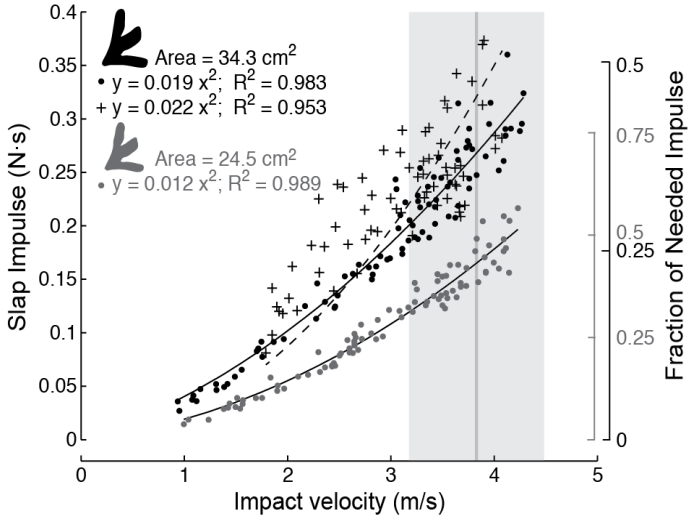

Figure 5. Impulse during slap phase of grebe foot models in comparison to a preserved grebe foot. The vertical slap impulse experienced by small (gray circles) and large (black circles) model grebe feet dropped into water in comparison to a fresh taxidermically prepared grebe foot (+ symbols). The prepared grebe foot had a flattened profile area of 34.2 cm^2, slightly smaller than the large grebe foot model. The coefficients of the best-fit quadratic regressions for the large model foot (solid black line) and large preserved foot (dashed black line) are not significantly different (p=0.77, two-tailed). The vertical gray bars correspond to the average +/- 1 s.e. of foot impact velocities recorded in the wild (3.83 ± 0.65 m/s). The right y-axis transforms slap impulse values to the fraction of impulse needed to support body weight, using a body mass of 1.44 kg for the large foot and 0.78 kg for the small foot.

Figure 6

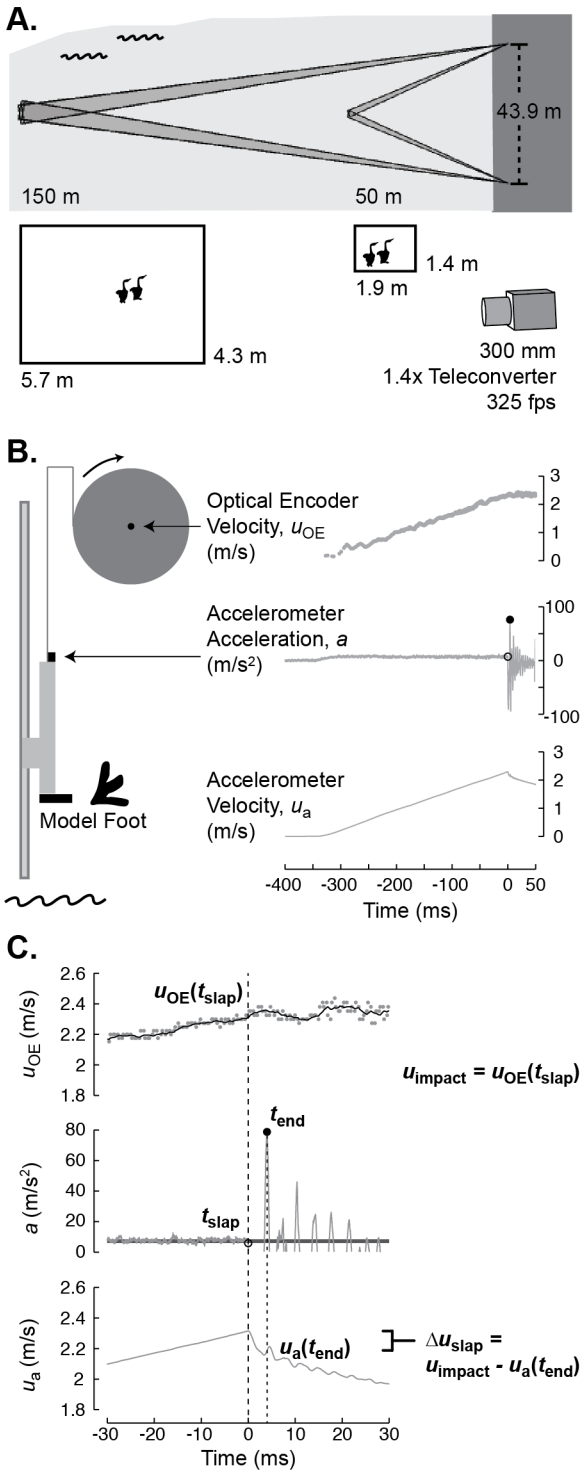
A.
43.9 m
150 m
50 m
1.4 m
1.9 m
4.3 m
5.7 m
300 mm
1.4x Teleconverter
325 fps
B.
Optical Encoder
Velocity, u_{OE}
(m/s)
Accelerometer
Acceleration, a
(m/s²)
Accelerometer
Velocity, u_a
(m/s)
Model Foot
Time (ms)
C.
$u_{OE}(t_{slap})$
$u_{impact} = u_{OE}(t_{slap})$
t_{end}
t_{slap}
$u_a(t_{end})$
$\Delta u_{slap} = u_{impact} - u_a(t_{end})$
Time (ms)

Figure 6. Experimental set-up of field recordings and foot slap laboratory protocol. (A) Schematic of high-speed videography set-up at Upper Klamath Lake, OR. Two high-speed cameras were separated by 43.9 m and focused on grebes ranging from 50-150 m away. (B) The set-up for slap impulse experiments and data from a typical trial. One of two 3D printed grebe feet was attached to the bottom of a small, "missile" section of 80/20 aluminum stock. A long vertical length of 80/20 ensured a consistent vertical drop. The foot missile was connected to a foam spool, which was attached to an optical encoder. The angular velocity was converted into the vertical drop velocity of the missile, u_{OE}. An accelerometer attached to the missile measured the missile acceleration, a, and velocity, u_a. (C) Method of extracting data for each slap impulse trial. The time of slap, t_{slap}, was determined as the first acceleration value outside one standard deviation of the average free fall acceleration (dark line in the acceleration record). The velocity at the time of slap impact, u_{impact}, was found from the filtered optical encoder velocity curve (moving average, N=5) and used to calibrate the accelerometer velocity profile. The end of slap period, t_{end}, was set as the largest positive value from the accelerometer trace. The velocity at the end of slap, $u_a(t_{end})$, was subtracted from u_{impact} to find the change in velocity of the missile during the slap phase.